Macromolecules

ARTICLE

pubs.acs.org/Macromolecules

Telechelic Hybrid Poly(acrylic acid)s Containing Polyhedral Oligomeric Silsesquioxane (POSS) and Their Self-Assembly in Water

Weian Zhang,*[,†] Jiayin Yuan,[‡] Stephan Weiss,[‡] Xiaodong Ye,[§] Chunliang Li,[§] and Axel H. E. Müller*[,‡]

[†]Department of Chemistry, East China University of Science and Technology, 130 Meilong Road, Shanghai 200237, China

[‡]Makromolekulare Chemie II, Universität Bayreuth, D-95440 Bayreuth, Germany

[§]Hefei National Laboratory for Physical Sciences at the Microscale and the Department of Chemical Physics, University of Science and Technology of China, Hefei, Anhui 230026, China

ABSTRACT: Telechelic ("dumbbell-shaped") POSS-containing inorganic/organic hybrid poly(*tert*-butyl acrylate) (POSS-P*t*BA-POSS) was prepared by the combination of ATRP and the copper-catalyzed azide−alkyne "click" reaction. Telechelic bromoterminated P*t*BAs with different molecular weights were first prepared via ATRP using a dibromo-functionalized ATRP initiator; subsequently, the bromo groups were transformed to azido groups using sodium azide in DMF via nucleophilic substitution. The "click" coupling between azido-terminated P*t*BA and alkyne-functionalized POSS was successfully accomplished to afford telechelic POSS-P*t*BA-POSS, which is confirmed by NMR and GPC. The telechelic POSS-P*t*BA-POSS was then hydrolyzed to amphiphilic telechelic POSS-functional poly(acrylic acid) (POSS-PAA-POSS). The self-assembly behavior of POSS-PAA-POSS with three different molecular weights in aqueous solution at pH 8.5 was investigated by transmission electron microscopy, scanning electron microscopy, and light scattering (SLS, DLS). The results show that POSS-PAA_{40}-POSS and POSS-PAA_{82}-POSS can self-assemble in water into ellipsoidal aggregates with a moderately uniform size, whereas POSS-PAA_{140}-POSS with a long PAA chain only self-assembles into aggregates with a broad size distribution. We discuss the formation of layered crystals of POSS within these aggregates.

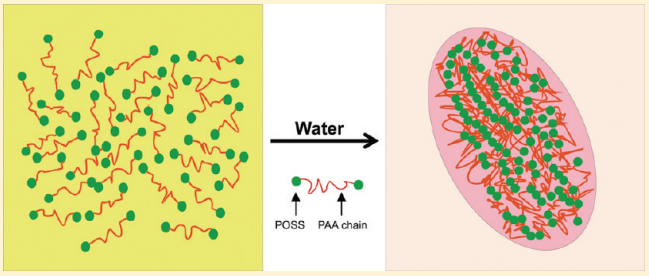

INTRODUCTION

During the past decade, the self-assembly of polymers, especially amphiphilic block copolymers, has received considerable attention because these assemblies show a rich variety of morphologies such as spheres, vesicles, cylinders, lamellae, and gyroids in bulk or in solution.[1−8] These morphologies can be controlled via the polymer type, structure, external stimuli (temperature, pH, etc.), solvent, additives (nanoparticles, salts, polymers, etc.), and many other factors. However, these self-assembly morphologies have mostly been formed from pure organic polymers, and the self-assembly behavior of hybrid polymers containing inorganic components has been rarely reported.[9−11]

Polyhedral oligomeric silsesquioxanes (POSS), as nanoscale enhancing agents, have been widely applied in the preparation of the polymer hybrids. The most common variety consists of eight $RSiO_{1.5}$ units forming a cage-like inorganic core surrounded by eight organic corner groups. Thus, POSS can be easily incorporated into polymeric matrices to prepare novel polymer hybrids by physical blending or chemical copolymerization.[12−26] Nowadays, with the emergence of new polymerization techniques such as living/controlled radical polymerization, some novel POSS-containing polymers with well-defined structures have been synthesized, and the self-assembly behavior of these hybrid polymers has also attracted great attention. For example, POSS methacrylate as a monomer was incorporated into polymer matrices by random copolymerization to prepare POSS-containing random copolymers, and an ordered nanostructure was obtained from the random copolymers.[27] POSS-containing diblock copolymers were also prepared by anionic polymerization, and lamellar self-assembly structures were observed in bulk.[28] POSS-containing ABA triblock copolymers were also synthesized via ATRP, and the self-assembly structure formed in thin films was investigated.[29,30] POSS molecules were also used to modify polystyrene-*block*-polybutadiene-*block*-polystyrene (SBS) triblock copolymers, and the self-assembly morphologies of the block copolymers were still preserved.[31,32] POSS was attached to the end of the polymer chain to prepare endfunctional ("monochelic") hybrid polymers, and the self-assembly of these hybrid polymers was also studied.[33−36] We prepared "tadpole-shaped" (monochelic) hybrid poly(*N*-isopropylacrylamide) (PNIPAAm) and poly(acrylic acid) using reversible addition−fragmentation transfer (RAFT) polymerization.[37,38] The tadpole-shaped POSS-PAAs self-assemble into rather large aggregates where the POSS moieties are dispersed in the particle. Recently, Cheng et al. prepared an inverse polymer,

Received: May 19, 2011
Revised: July 28, 2011
Published: August 10, 2011

POSS-containing tadpole-shaped polystyrene with a hydrophilic POSS as the "head", and obtained interesting self-assembly morphologies in different solutions.[39]

In this contribution, we continue the study of the self-assembly of POSS-containing hybrid polyelectrolytes. "Dumbbell-shaped", POSS-containing telechelic poly(*tert*-butyl acrylate) (POSS-P*t*BA-POSS) was prepared by the combination of ATRP and "click chemistry".[40] The telechelic POSS-P*t*BA-POSS was further hydrolyzed into POSS-containing telechelic poly(acrylic acid) (POSS-PAA-POSS) using trifluoroacetic acid (TFA). The self-assembly behavior of the telechelic amphiphilic POSS-PAA-POSS was investigated by transmission electron microscopy (TEM), scanning electron microscopy (SEM), and light scattering (LS).

EXPERIMENTAL SECTION

Materials. Aminoisobutyl polyhedral octameric silsesquioxane (POSS) was purchased from Hybrid Plastics Company. *tert*-Butyl acrylate (*t*BA) was kindly supplied by BASF SE and was passed through a silica column to remove the inhibitor shortly before polymerization. CuBr was purified by stirring with acetic acid overnight. After filtration, it was washed with ethanol and ether and then dried in a vacuum oven at room temperature overnight. Triethylamine and dichloromethane were, respectively, dried over CaH_2 and distilled prior to use. Tetrahydrofuran (THF) was distilled from a purple sodium ketyl solution.

Preparation of 3-Propargyl carbonyl-*N*-[3-(isobutyl polyhedral oligomeric silsesquioxane) propyl]propanamide (Alkyne-POSS)¶. The preparation of alkyne-POSS has been reported in our previous paper.[40] ^{1}H NMR ($CDCl_3$, ppm): 4.71 (d, *2H*, $-COOCH_2CCH$,), 3.26 (q, *2H*, $-Si-CH_2CH_2CH_2NH-$), 2.75 (t, *2H*, $-NHCOCH_2CH_2COO-$), 2.50 (m, *3H*, $-NHCOCH_2CH_2COO-$, $-COOCH_2CCH$), 1.87 (m, *7H*, $-Si-CH_2CH(CH_3)_2$), 1.61 (m, *2H*, $-Si-CH_2CH_2CH_2NH-$), 0.98 (d, *42H*, $-Si-CH_2CH(CH_3)_2$), 0.62 (q, *16H*, $-Si-CH_2CH(CH_3)_2$, $-Si-CH_2CH_2CH_2NH-$).

Preparation of 1,4-Bis(2-bromoisobutylcarbonyloxy)-butane (BiBB). A round-bottomed flask (250 mL) equipped with a magnetic stir bar was charged with 1,4-butanediol (3.0 g, 0.033 mol), triethylamine (13.92 mL, 0.10 mol), and anhydrous THF (120 mL). After stirring for 20 min at 0 °C, 2-bromo-2-methylpropionylbromide (12.34 mL, 0.10 mol) in 30 mL of anhydrous THF was slowly added under argon. After stirring for 24 h at ambient temperature, the reaction mixture was filtered, and the solvent was removed in vacuo. The resulting mixture was dissolved in dichloromethane and, respectively, washed with a saturated solution of $NaHCO_3$ and NaCl, the organic layer was dried over anhydrous $MgSO_4$ and concentrated in vacuo. Finally, the crude product was crystallized in toluene twice, and 9.68 g of white crystal was obtained with 75% yield. ^{1}H NMR ($CDCl_3$-*d* ppm): 4.24 (m, *4H*, $-OCH_2(CH_2)_2CH_2O-$), 1.94 (s, *12H*, $Br(CH_3)_2$-$CO-$,$-OC(CH_3)_2Br$), 1.83 (m, *4H*,$-OCH_2(CH_2)_2CH_2O-$).

Preparation of Dibromo-Terminated P*t*BA (Br-P*t*BA-Br) Using ATRP. A round-bottomed glass flask (25 mL) charged with a magnetic stir bar, *t*BA (6.80 mL, 0.047 mol), BiBB (1.74 g, 0.45 mmol), CuBr (0.032 g, 0.22 mmol), acetone (1.5 mL), and toluene (0.50 mL) was purged with argon. After 20 min, PMDETA (0.047 mL, 0.22 mmol) was added under argon, and the flask was purged with argon for another 5 min. The polymerization was carried out at 60 °C. Small samples (~0.05 mL) were taken out from the reaction flask at intervals to check the conversion, which was measured by ^{1}H NMR by comparing the peaks of the double-bond protons at 5.78 ppm and those of the toluene aromatic protons at 7.29 ppm. At the end of the polymerization reaction, the reaction solution obviously became viscous. Final conversion determined by ^{1}H NMR reached 84%. The reaction was stopped by cooling to room temperature and opening to the air, and THF was added. After passing through a basic alumina column, the solution was concentrated by a rotary evaporator. Afterward, it was precipitated into a mixed solution of water/methanol (v/v, 1/4) to remove the residual monomer and other impurities. The polymer was dried under vacuum at 50 °C for 24 h (M_n = 10 880 g/mol, M_w/M_n = 1.30).

Preparation of Diazido-Terminated P*t*BA (N_3-P*t*BA-N_3). A round-bottomed glass flask (20 mL) with a magnetic stirring bar was charged with Br-P*t*BA-Br (1.50 g, 0.14 mmol), sodium azide (0.18 g, 2.8 mmol), and DMF (10 mL). The solution was allowed to stir overnight at room temperature. At the end of the reaction, the solution was precipitated into a mixed solution of water/methanol (v/v 1/4). The resulting product was filtered and dried at 50 °C for 24 h to give 1.28 g of N_3-P*t*BA-N_3, 85.0% yield.

Preparation of Telechelic POSS-Containing P*t*BA Hybrids (POSS-P*t*BA-POSS) via CuBr-Catalyzed Click Coupling. A round-bottomed glass flask (20 mL) charged with a magnetic stirring bar, N_3-P*t*BA_{82}-N_3 (0.60 g, 0.056 mmol), alkyne-POSS (0.33 g, 0.34 mmol), PMDETA (0.23 mL, 1.1 mmol), and DMF (10 mL) was purged with argon. After 20 min, CuBr (0.16 g, 1.1 mmol) was added under argon, and the flask was purged with argon for another 5 min. The reaction was carried out at 80 °C. After 24 h, the flask was opened, and THF was added to quench the reaction. The solution was passed through a basic alumina column. The solution was diluted into 50 mL and dialyzed in THF using a dialysis membrane (MWCO = 12 000−14 000). After 7 days, the unreactive alkyne-POSS was completely removed. The resulting product was dried under vacuum at 50 °C for 24 h (0.54 g, yield 82%). M_n = 14 400, M_w/M_n = 1.21.

Preparation of POSS-PAA-POSS. A round-bottomed flask (50 mL) with a magnetic stir bar was charged with POSS-P*t*BA_{82}-POSS (0.4 g, 2.7 mmol of *t*BA unit), followed by dichloromethane (40 mL). The mixture was allowed to stir for 15 min to dissolve the polymer. Then, TFA (3.0 mL, 40.0 mmol) was added. The mixture was allowed to stir at room temperature. After 24 h, dichloromethane and TFA were removed by a rotary evaporation. The product was washed three times with dichloromethane, redissolved, and freeze-dried from dioxane. M_n = 6217, M_w/M_n = 1.11 (MALDI-TOF).

Self-Assembly of POSS-PAA-POSS in Aqueous Solution. A typical self-assembly aggregate solution of telechelic POSS-PAA-POSS was prepared as that of monochelic POSS-PAA.[38] POSS-PAA_{82}-POSS (20 mg) was first dissolved in dioxane (5 mL). The solution was stirred overnight and gradually dialyzed against pH 8.5 Millipore water (resistance = 18 MΩ) for 3 days. After gradual dialysis, the self-assembly solution was dialyzed at least three times using pH 8.5 Millipore water to make sure to remove dioxane completely. The critical micelle concentration (CMC) of POSS-PAA_{82}-POSS in water is 2.4 mg/L, as determined by the fluorescent probe technique with pyrene as a probe.[41]

CHARACTERIZATION

Nuclear Magnetic Resonance (NMR) Spectroscopy. The ^{1}H NMR and ^{13}C NMR measurements were carried out on a Bruker AC-250 instrument. The samples were dissolved with deuterated $CDCl_3$ or dioxane-d_8, and measured with tetramethylsilane (TMS) as an internal reference.

^{29}Si NMR spectra were measured on a Varian Inova 300 MHz spectrometer at 23 °C. The samples were dissolved in dioxane-d_8; chemical shifts are given relative to TMS [δ^{29}Si = 0 ppm for $\Xi(^{29}Si)$ = 19.867184 MHz]; Chemical shifts are given to ±0.1 for ^{29}Si; coupling constants are given ±0.4 Hz for $J(^{29}Si)$. The spectra were measured by using the refocused INEPT pulse sequence based on $^{2/3}J(^{29}Si)$ = 10 Hz after optimizing the delay times in the pulse sequence.

Fourier Transform Infrared Spectroscopy. Fourier Transform Infrared Spectroscopy (FTIR) measurements were conducted on a Perkin-Elmer Spectrum One FT-IR spectrophotometer equipped with an ATR sampling unit (25 °C).

Gel Permeation Chromatography. The molecular weights and molecular weight distribution were measured by conventional gel permeation chromatography (GPC). Column set: 5 μm SDV gel, 10^2, $10^{3,}$ 10^4, and 10^5 Å, 30 cm each (PSS, Mainz). Detectors used are RI and UV operated at 254 nm. Polystyrene standards (PSS, Mainz) with narrow molecular weight distribution were used for the calibration of the column set, and THF was used as the eluent at a flow rate of 1 mL/min.

MALDI-TOF Mass Spectrometry. MALDI-TOF mass spectrometry was performed on a Bruker Reflex III instrument equipped with a 337 nm N_2 laser in the reflector mode and 20 kV acceleration voltage. 2,5-Dihydroxybenzoic acid (Aldrich, 97%) was used as a matrix. Samples were prepared from dioxane solution by mixing matrix (20 mg/mL) and polymer (10 mg/mL) in a ratio of 4:1. The number-average molecular weights of the polymers were determined in the linear mode.

Transmission Electron Microscopy. TEM images were taken on a LEO 922 OMEGA electron microscopes operated at 200 kV. A 5 μL droplet of self-assembly aggregate solution (1 mg/mL) was directly dropped onto a copper grid (300 mesh) coated with a carbon film, followed by drying at room temperature.

Scanning Electron Microscopy. SEM was performed using a LEO 1530 Gemini instrument equipped with a field emission cathode with a lateral resolution of ~2 nm. The acceleration voltage was chosen between 0.5 and 3 kV.

Wide-Angle X-ray Diffraction. Wide-angle X-ray diffraction (WAXD) patterns were recorded in transmission with a Bruker D8 Advance X-ray diffractometer. The wavelength used was Cu Kα (λ = 0.154 nm), and spectra were recorded in the 2θ range of 4−40° (step size 0.025°).

Static and Dynamic Light Scattering. Static and dynamic light scattering (SLS, DLS) were measured on a DLS/SLS-5022F instrument (ALV Germany) equipped with a multi-τ digital time correlation (ALV5000) and a cylindrical 22 mW UNIPHASE He−Ne laser (λ_0 = 632 nm) as the light source. In SLS,[42,43] the angular dependence of the absolute excess time-average scattering intensity, known as the Rayleigh ratio, $R_{vv}(q)$, is found, and we can obtain the weight-average molar mass, M_w, the root-mean-square radius of gyration, $\langle R_g^2 \rangle_z^{1/2}$ (or written as $\langle R_g \rangle$), and the second virial coefficient, A_2, by using the Zimm equation. The refractive index increment (dn/dC = 0.044 mL g^{-1}) of POSS-PAA_{82}-POSS aggregates was determined with a precise differential refractometer at 25 °C and 633 nm.[44]

In DLS,[45] the intensity−intensity time correlation function $G^{(2)}(t,q)$ in the self-beating mode results in a decay time distribution $G(\Gamma)$. For diffusive relaxation, Γ is related to the translational diffusion coefficient, D, of the scattering object (polymer chain or colloid particle) in dilute solution or dispersion by $(\Gamma/q^2)_{q\to 0,C\to 0} = D$ and further to the hydrodynamic radius, R_h, by the Stokes−Einstein equation. All solutions were filtered through a 0.45-μm PTFE Millipore filter.

RESULTS AND DISCUSSION

In our previous work, we prepared monofunctional ("tadpole-shaped", "monochelic") POSS-PAA via RAFT polymerization using a POSS-containing RAFT agent. It was found that

Scheme 1. Synthesis of Telechelic POSS-PAA-POSS by a Combination of ATRP and "Click Chemistry"

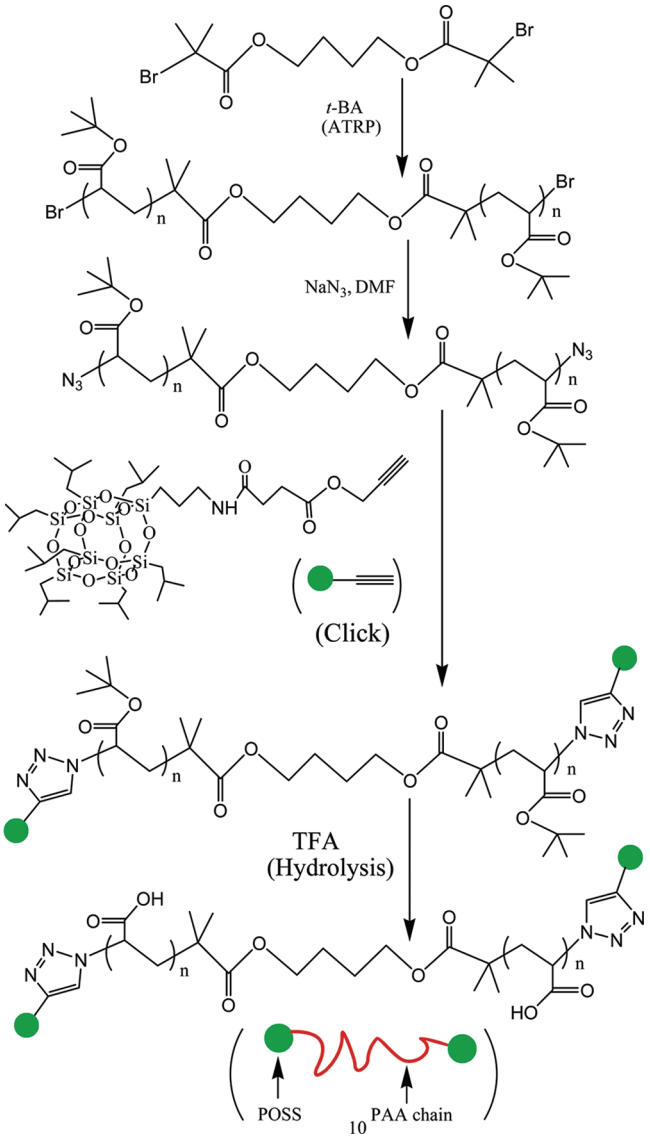

amphiphilic POSS-PAA self-assembles in water into aggregates of different size, where the POSS moieties are dispersed in the aggregates. This is very different from a conventional core−shell micelle with hydrophobic POSS molecules as the core and hydrophilic PAA as the shell.[38] To further explore the self-assembly morphologies and mechanism of POSS-containing polyelectrolytes, we synthesized telechelic ("dumbbell-shaped") POSS-PAA-POSS, where two ends of the PAA chain are attached to POSS. The synthetic strategy is shown in Scheme 1. The synthesis was performed in four main steps. Telechelic dibromo-terminated P*t*BA (Br-P*t*BA-Br) with different molecular weights was first prepared via ATRP using a dibromo-functionalized initiator; subsequently, the terminal bromo groups were transformed to azido groups using sodium azide in DMF via nucleophilic substitution. Then, the click coupling occurred between the α,ω-diazido-P*t*BA (N_3-P*t*BA-N_3) and the alkyne-functionalized POSS (alkyne-POSS) to afford telechelic POSS-P*t*BA-POSS. Finally, the POSS-containing polyelectrolyte, telechelic

Table 1. Results of Polymerization of *t*BA at 60 °C

sample	$[M]_0/[I]_0$[a]	$M_{n,GPC}$[b]	$M_{n,th}$[c]	M_w/M_n[b]	x (%)
Br-P*t*BA$_{40}$-Br	55	5460	6060	1.30	86
Br-P*t*BA$_{82}$-Br	104	10 900	11 600	1.30	84
Br-P*t*BA$_{140}$-Br	156	18 300	18 00	1.29	90

[a] $[M]_0$ = 4.7 M. [b] Determined by GPC using polystyrene standards. [c] Theoretical number-average molecular weight, $M_{n,th} = [M]_0/[I]_0 \times M_{tBA} \times x + M_{init}$, where M_{tBA} and M_{init} are the molecular weights of *t*BA and initiator, respectively, and x is the conversion, as measured by ^{1}H NMR.

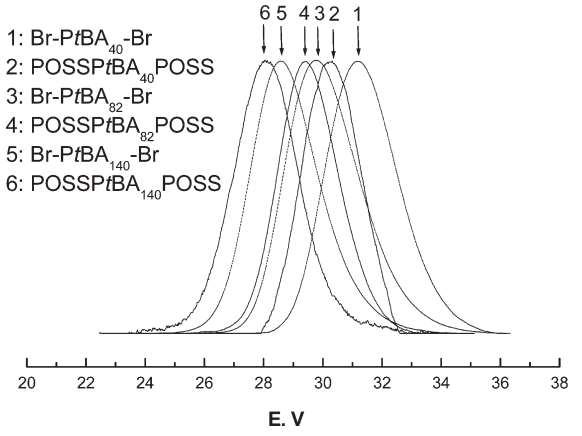

Figure 1. Evolution of GPC chromatograms of Br-P*t*BA-Br and POSS-P*t*BA-POSS of different molecular weights.

POSS-PAA-POSS, was obtained by hydrolysis of POSS-P*t*BA-POSS using TFA.

The telechelic Br-P*t*BA-Br was synthesized at 60 °C by ATRP using CuBr/PMEDTA as the catalyst. The reaction conversion was determined by ^{1}H NMR by comparing the peaks of the double-bond protons at 5.75 ppm with those of aromatic protons at 7.23 ppm. The reaction was quenched at a desired conversion of *t*BA. The molecular weights and PDIs of the P*t*BA polymers are listed in Table 1. The low polydispersity and well-symmetrical GPC curves (Figure 1) indicate that the polymerization of *t*BA is well-controlled using a dibromo-functionalized ATRP initiator.

The terminal bromo groups of Br-P*t*BA-Br were transformed into azido groups to afford telechelic N_3-P*t*BA-N_3 by nucleophilic substitution. The reaction was performed in DMF for 24 h at room temperature. FT-IR was used to characterize the formation of terminal azido groups of N_3-P*t*BA$_{82}$-N_3 (Figure 2). Compared with the FT-IR spectrum of Br-P*t*BA$_{82}$-Br, a peak at 2111 cm^{-1} appears in the spectrum of N_3-P*t*BA-N_3, which is assigned to the stretching vibration of terminal azido groups. This indicates that the nucleophilic substitution was effectively conducted, and the terminal bromo groups were transformed to azido groups.

The azide/alkyne "click" coupling between N_3—P*t*BA$_{82}$-N_3 and alkyne-POSS was performed at 80 °C for 24 h in DMF using CuBr/PMDETA as catalyst. To complete the coupling reaction, the initial molar ratio of alkyne-POSS to N_3—P*t*BA$_{82}$-N_3 was set to be 3/1. The unreacted excess alkyne-POSS was removed via dialysis against THF.

Figure 3 shows the ^{1}H NMR spectrum of POSS-P*t*BA$_{82}$-POSS. Except for the characteristic signals at δ 2.25 (d) and

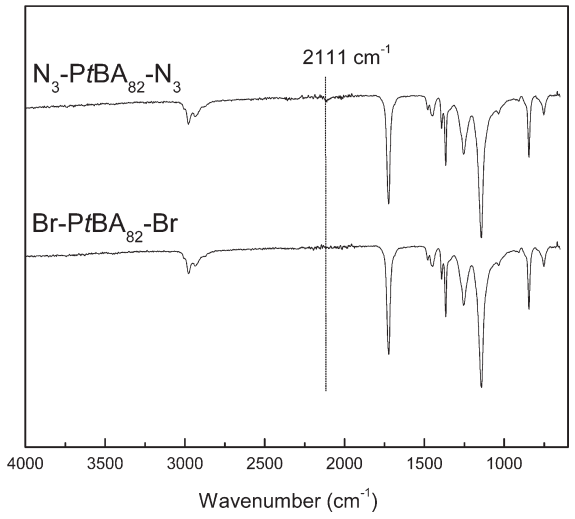

Figure 2. FT-IR spectra of Br-P*t*BA$_{82}$-Br and N_3-P*t*BA$_{82}$-N_3.

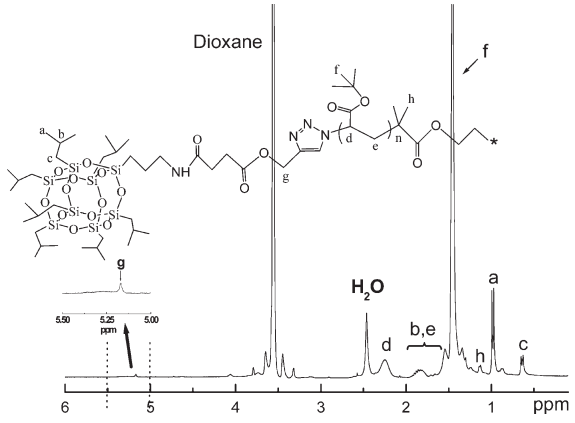

Figure 3. ^{1}H NMR spectrum of POSS-P*t*BA$_{82}$-POSS.

1.45 (f), respectively, ascribed to the methine protons of the backbone and the methyl protons of the *tert*-butyl groups of P*t*BA, the signals at δ 0.98 and 0.64 (c) are, respectively, assigned to the methyl protons ($-$Si-CH$_2$CH(CH_3)$_2$) and methylene protons ($-$Si-CH_2CH(CH$_3$)$_2$ and $-$Si-CH_2CH$_2$CH$_2$NH$-$) originating from alkyne-POSS. Moreover, it still can be discerned that the signal at δ 5.17 (g) is ascribed to the methylene protons adjacent triazole ring in the enlarged image of ^{1}H NMR spectrum. In addition, the FT-IR spectrum was also used to confirm the click reaction (Figure 4). Compared with the FT-IR spectrum of N_3-P*t*BA$_{82}$-N_3, the peak at 2111 cm^{-1} of azide stretching vibration completely disappeared, and a new peak appeared at 1114 cm^{-1} in the spectrum of POSS-P*t*BA$_{82}$-POSS, which is assigned to the stretching vibration of Si-O-Si.

The GPC traces of POSS-P*t*BA-POSS with different molecular weights are shown in Figure 1. All curves of POSS-P*t*BA-POSS shift to lower elution volume compared with those of their maternal Br-P*t*BA-Br. Moreover, the traces are well symmetrical, and no shoulder and tail appears. This confirms the click coupling is complete.

Preparation of POSS-PAA-POSS from POSS-P*t*BA-POSS Using TFA. POSS-PAA-POSS was obtained by hydrolysis of the *tert*-butyl ester groups of POSS-P*t*BA-POSS in dichloromethane using TFA. TFA, as an organic acid, is frequently

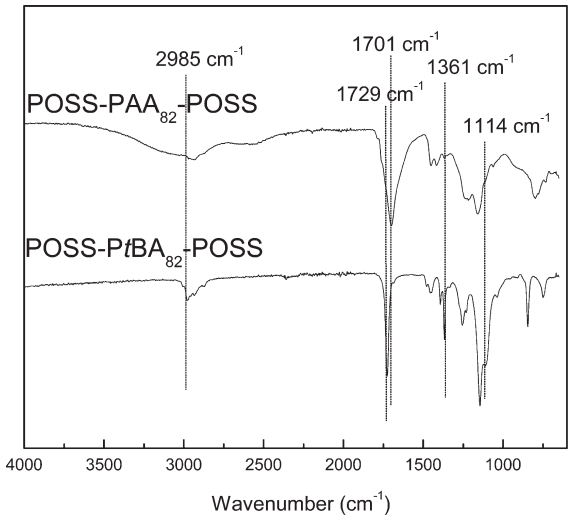

Figure 4. FT-IR spectra of POSS-P*t*BA$_{82}$-POSS and POSS-PAA$_{82}$-POSS.

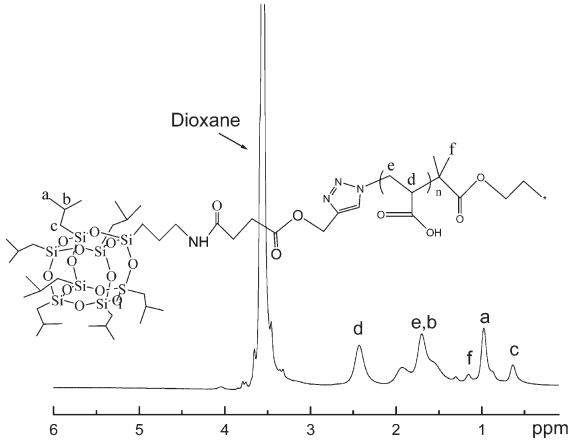

Figure 5. ^{1}H NMR spectrum of POSS-PAA$_{82}$-POSS.

applied in organic reactions instead of hydrochloric acid because of its good solubility in organic solvent. Previous literature had reported that the triazole ring and silsesquioxane (POSS) are stable in TFA solution.[38,46−49] The FT-IR spectrum of POSS-PAA$_{82}$-POSS is shown in Figure 4. Compared with the FT-IR spectrum of POSS-P*t*BA$_{82}$-POSS, we can find a broad absorption band appearing in the range from 2260 to 3662 cm^{-1} in the spectrum of POSS-PAA$_{82}$-POSS. The carbonyl peak at 1729 cm^{-1} is slightly shifted to lower wave numbers at 1701 cm^{-1}, and the peak also became broader. These are due to the formation of carboxylic acid groups from the *tert*-butyl ester. In addition, the deformation vibration of the *tert*-butyl group at 1361 cm^{-1} completely disappeared in the IR spectrum of POSS-PAA$_{82}$-POSS. This suggests that the hydrolysis is complete.

^{1}H, ^{13}C, and ^{29}Si NMR was also used to characterize the formation of POSS-PAA$_{82}$-POSS. Figure 5 shows that the proton signal of the *tert*-butyl ester groups at 1.45 ppm completely disappeared, and the characteristic proton signals of POSS are almost unchanged at δ 0.98 (a) and 0.63 (c). The ^{13}C NMR spectrum also shows that the carbon resonance for the *tert*-butyl ester at 27.87 and 80.17 ppm in spectrum of POSS-P*t*BA-POSS completely disappeared in the spectrum of POSS-PAA$_{82}$-POSS.

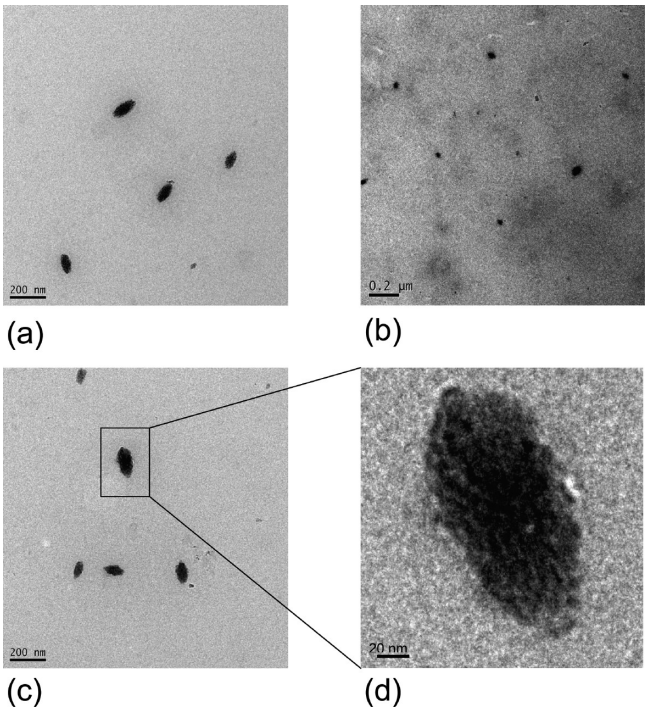

Figure 6. TEM of POSS-PAA-POSS self-assembly aggregates drop-coated from water at pH 8.5 and C = 1.0 mg/mL. (a) POSS-PAA$_{40}$-POSS, (b) POSS-PAA$_{140}$-POSS, and (c,d) POSS-PAA$_{82}$-POSS. Scale bars = 200 (a−c), 20 nm (d).

The ^{29}Si NMR spectrum shows that the characteristic silicon resonances of POSS are still at δ −63.8 and −64.1 after hydrolysis. Therefore, on the basis of the FTIR and NMR results, POSS-PAA$_{82}$-POSS was successfully prepared from the hydrolysis of POSS-P*t*BA$_{82}$-POSS. In addition, the molecular weight of POSS-PAA$_{82}$-POSS measured by MALDI-TOF mass spectrometry is close to the theoretically calculated one, which further confirms that POSS-PAA$_{82}$-POSS was successfully prepared.

Self-Assembly Behavior of Telechelic POSS-PAA-POSS. In past reports on the self-assembly of POSS-containing hybrid polymers, the self-assembly morphologies were mostly studied in bulk. For example, a lamellar self-assembly nanostructure can be obtained from POSS-containing random or block copolymers.[27,28] There are rare reports on the self-assembly behavior of POSS-containing hybrid polymers in solution. In our previous work, we synthesized tadpole-shaped ("monochelic") POSS-endfunctional poly(acrylic acid) (POSS-PAA) via RAFT polymerization and found the self-assembly behavior to be different from that of the well-known organic amphiphilic block copolymers such as polystyrene-*block*-poly(acrylic acid) (PS-*b*-PAA).[50,51] POSS-PAA in water only formed rather large, spherical aggregates, a self-assembly structure obviously different from the well-known core−shell micelles with the hydrophobic block as the core and the hydrophilic block as the shell. To study further the self-assembly behavior of POSS-containing amphiphilic hybrid polyelectrolytes in water, we synthesized telechelic POSS-PAA-POSS, and unusual self-assembly morphologies were expected. TEM was carried out to characterize the self-assembly morphologies of the POSS-PAA-POSS in water. The sample for TEM was prepared by applying a drop of the polymer solution on a carbon-coated copper grid without additional staining or etching.

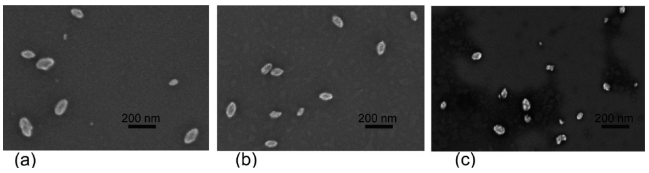

Figure 7. SEM images of POSS-PAA-POSS self-assembly aggregates from water at pH 8.5 and C = 1.0 mg/mL. (a) POSS-PAA$_{40}$-POSS, (b) POSS-PAA$_{82}$-POSS, and (c) POSS-PAA$_{140}$-POSS. Scale bars = 200 nm.

Figure 6 shows TEM images obtained from aqueous solutions of POSS-PAA-POSS at pH 8.5. Surprisingly, the self-assembly aggregates of POSS-PAA$_{40}$-POSS (Figure 6a) are rather large ellipsoids, obviously different in shape from the previous self-assembled monochelic POSS-PAA.[38] The major axis (longest diameter) of the ellipsoids is 100−150 nm, and the minor axis (shortest diameter) is 50−75 nm. POSS-PAA$_{82}$-POSS, despite a longer PAA chain, shows a similar morphology and size (Figure 6c). Only POSS-PAA$_{140}$-POSS shows a more spherical morphology. Because the aggregates are much larger than the contour length of PAA, which is only 10−35 nm, they must have a more complicated structure than a conventional micelle. The shape and size of the self-assembly morphologies of telechelic POSS-PAA-POSS is confirmed by SEM (Figure 7).

To observe the structure of the self-assembly ellipsoids in more detail, we enlarge a single ellipsoid image in Figure 6d. We find that the contrast density within the ellipsoid is inhomogeneous, namely with dark domains dispersed in the ellipsoid. The dark domains are attributed to the POSS aggregates, which seem to form chain-like or lamellar structures parallel to the long axis. Apparently, aggregates or crystals of POSS are embedded in a PAA matrix. Mesoscale aggregates of micelles (sizes of hundreds of nanometers) have been frequently observed in the literature, but typically, these are of spherical shape and do not show a similar fine structure[52]

Zhang and Eisenberg observed ellipsoidal large compound micelles of very asymmetric polystyrene$_{200}$-*b*-PAA$_4$.[53] Lodge and Hillmyer et al. reported that self-assembly ellipsoids can be formed from amphiphilic poly(ethylene oxide)-*b*-polystyrene-*b*-1,2-polybutadiene ABC triblock terpolymers.[54,55] First, the triblock terpolymers self-assembled into spherical micelles with two hydrophobic blocks as the core. The ellipsoidal morphologies were then formed by fluorination of one block, which induced internal segregation into an inner core and an intermediate shell. Khokhlov et al. prepared asymmetric diblock copolymers by introducing a small amount of a polar group, such as a zwitterionic group, at either end of polymer chain, and they revealed two separate levels of microphase separation.[56] They also synthesized a polystyrene-*block*-poly(sodium methacrylate)-*block*-polystyrene (PS$_{7.1}$-*b*-PMA$_{211}$-*b*-PS$_{7.1}$) ABA triblock copolymer, which has a similar structure to POSS-PAA-POSS. They studied the aggregation behavior of the block copolymer in aqueous solution and found macroscopic phase separation, even a macroscopic gel formed at higher polymer concentration, and no micelles or ellipsoidal aggregates.[57]

In our present study, we assume that two reasons account for the formation of the self-assembly ellipsoids. First, POSS tends to form layer crystals at a higher amount of POSS aggregates because POSS contains an inorganic core. Coughlin et al. found that POSS very easily forms layer crystals in random copolymers of polybutadiene and poly(POSS-norbornene).[27]

Scheme 2. Self-Assembly Process of Telechelic POSS-PAA-POSS in Water

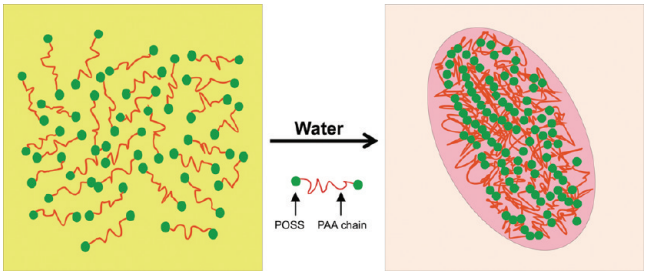

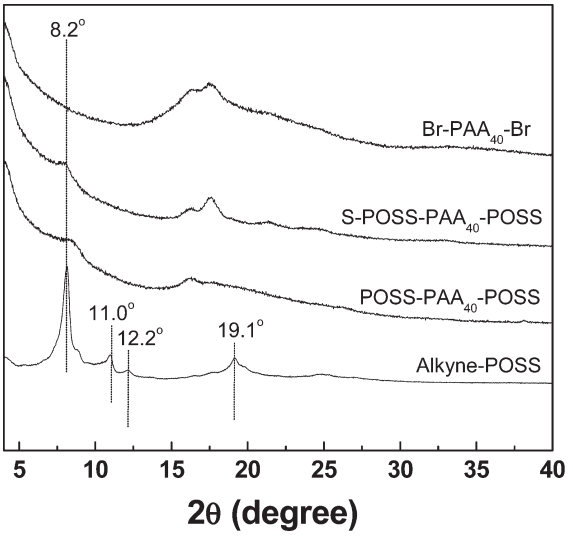

Figure 8. X-ray diffraction patterns of alkyne-POSS, POSS-PAA$_{40}$-POSS in bulk and freeze-dried aggregates, respectively, and pure PAA$_{40}$.

When the amount of POSS aggregates is only 12%, some short randomly oriented layer crystals form in the hybrid random copolymers, which is similar to the exfoliated structure of polymer/clay nanocomposites.[58] When the amount of POSS aggregates increases to 43%, obvious lamellar structure forms. Zhu et al. also found similar morphologies in DNA/POSS hybrids. In our research, the amount of POSS in the telechelic POSS-PAA$_{82}$-POSS is ∼27%, and POSS is expected to be capable to form layer crystals. A close view of the enlarged ellipsoid in Figure 6d indicates that some POSS aggregates connect to each other, tending to a layered irregular structure. According to this observation, we believe that the capability of the POSS aggregates to form layered crystal is the main driving force in the formation of ellipsoids. Correspondingly, a schematic illustration is shown in Scheme 2.

To confirm our assumption, we conducted WAXD measurements (Figure 8). The diffraction peaks of alkyne−POSS, respectively, show diffraction peaks at 2θ = 8.2 (1.08 nm), 11.0 (0.80 nm), 12.2 (0.72 nm), and 19.1° (0.46 nm), which are associated with the hexagonal crystalline structure of POSS.[59] For POSS-PAA$_{40}$-POSS, the diffraction peak at 8.2° becomes weak, and the other diffraction peaks derived from POSS could not clearly be discerned because of the overlapping of the wide dispersion peak of the PAA amorphous phase. This indicates that POSS aggregates into crystals in the bulk of telechelic

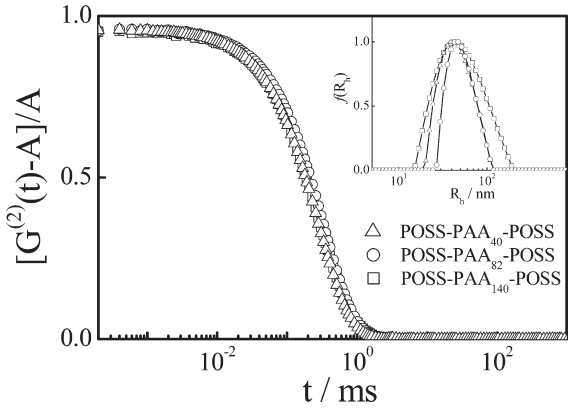

Figure 9. Typical measured intensity−intensity time correlation function, $[G^{(2)}(t,q) - A]/A$, for telechelic POSS-PAA-POSS self-assembly aggregates at 90° ($q = 1.86 \times 10^7$ m^{-1}). The inset shows corresponding intensity-weighted hydrodynamic radius distributions, $f(R_h)$.

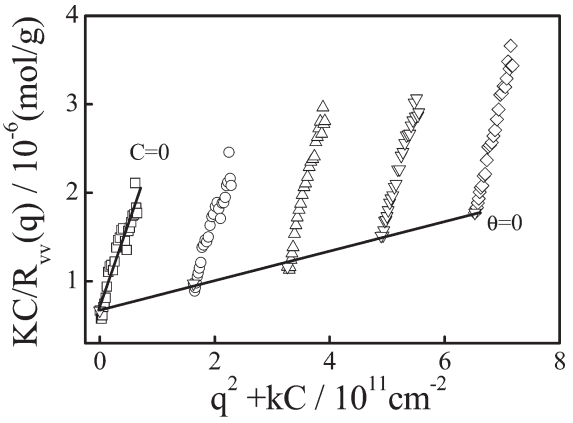

Figure 10. Typical Zimm plot of POSS-PAA$_{82}$-POSS in aqueous solution at T = 25 °C, pH 8.5, where the concentration ranged from 5.0×10^{-4} to 2.0×10^{-3} g/mL and $k = 3.264 \times 10^{14}$.

POSS-PAA$_{40}$-POSS. To obtain the sample of the self-assembly aggregates (denoted with "S"), the solution with C = 1.0 mg/mL was freeze-dried for 24 h. It can be seen that the dispersion peak of the PAA amorphous phase becomes strong because the shell of the aggregates is mostly composed of PAA. However, diffraction peak at 8.2° has comparable intensity. This confirms that POSS aggregates into larger crystals after self-assembly in water. On the basis of the XRD result, POSS is in a crystalline state dispersed in the aggregates.

In the enlarged image of the single ellipsoid (Figure 6d), we find that the POSS tends to aggregate into layered structures, although not perfectly. Moreover, the density of the POSS in the domain of the POSS aggregates is not uniform. This is related to the special telechelic structure. Although telechelic POSS-containing PAA has similar ratios of POSS/PAA as monochelic POSS-PAA studies before,[38] the entanglement between two PAA chains can easily occur in the self-assembly process, and the entanglement of the PAA chains perhaps prevents the POSS aggregates from growing larger.

The self-assembly behavior of POSS-PAA$_{140}$-POSS with a longer PAA chain was also studied. From Figures 6b and 7c, it appears that the self-assembly morphology of POSS-PAA$_{140}$-POSS is a transition between spheres and ellipsoids. Moreover, the size of aggregates has a wide dispersity from 30 to 120 nm. For longer PAA chains, the POSS content decreases, and we assume that this hinders the formation of layered crystals, like the case of the monochelic POSS-PAA. Additionally, the entangling interaction will modify the self-assembly behavior of POSS-PAA$_{140}$-POSS compared with that of the monochelic POSS-PAA so that it can self-assemble into irregular aggregates

The self-assembly aggregates in aqueous solution at pH 8.5 were also characterized by LS. DLS measured at 90° (scattering vector $q = 1.86 \times 10^7$ m^{-1}) shows the apparent hydrodynamic radius $\langle R_h \rangle$ of all aggregates are in the range 43−47 nm, which is agreement with the average of the major and minor radii measured by TEM (Figure 9). The cumulant analysis renders rather large polydispersities, PDI = 0.081 and 0.115, respectively, for POSS-PAA$_{82}$-POSS and POSS-PAA$_{40}$-POSS. For POSS-PAA$_{140}$-POSS, the polydispersity is even higher, PDI = 0.243, which agrees with the results of TEM and SEM. The corresponding intensity-weighted hydrodynamic radius distribution in the inset of Figure 9, calculated from the Laplace inversion of a corresponding intensity−intensity time correlation function using the CONTIN program, also shows that POSS-PAA$_{140}$-POSS aggregates have a higher polydispersity. Considering the effect of measurement angle on $\langle R_h \rangle$, we measured the scattering vector, q, dependence of the decay rate, Γ. The results (not shown) revealed that Γ is well linearly dependent on q^2, indicating that the aggregates have a diffusive behavior. With q in the range from (2.3 to 6.5) $\times 10^{14}$ m^{-2}, DLS measurements show that $D = 4.9 \times 10^{-12}$ m^2/s. The calculated $\langle R_h \rangle$ is 45 nm, which is close to 47 nm measured at 90°. The measured hydrodynamic radii are significantly smaller than those of POSS-PAA$_x$ (x = 65−136), which were in the range of 60−65 nm, except for POSS-PAA$_{35}$, which had $\langle R_h \rangle$ = 46 nm. Moreover, all POSS-PAA aggregates were much more polydisperse (PDI = 0.3 to 0.5). Therefore, telechelic POSS-containing PAA has a higher tendency to form aggregates with a uniform size, in particular, for short PAA blocks.

Figure 10 shows a typical Zimm plot for the SLS of POSS-PAA$_{82}$-POSS in aqueous solution. The extrapolation of $[KC/R_{vv}(q)]$ to $q \rightarrow 0$ and $C \rightarrow 0$ leads to the value of $M_w = 1.43 \times 10^6$ g/mol, whereas the slopes for the lines plotting $[KC/R_{vv}(q)]_{C \rightarrow 0}$ versus q^2 and $[KC/R_{vv}(q)]_{q \rightarrow 0}$ versus C give the values of $\langle R_g \rangle$ = 92 nm and $A_2 = (2.74 \pm 0.23) \times 10^{-4}$ mol·mL·g^{-2}, respectively. The small values of A_2 imply that water is a selective solvent for the aggregates. The aggregation number, N_{agg}, can be calculated using $N_{agg} = M_{w,micelle}/M_{w,blockcopolymer}$. The calculated aggregation number of POSS-PAA$_{82}$-POSS in aqueous solution is $N_{agg} \approx 180$.

CONCLUSIONS

Inorganic/organic hybrid telechelic POSS-PAA-POSS was successfully prepared by the combination of ATRP and "click chemistry". The self-assembly behavior of POSS-PAA-POSS with three different molecular weights in aqueous solution at pH 8.5 was investigated by TEM, SEM, and LS. Unexpectedly, POSS-PAA$_{40}$-POSS and POSS-PAA$_{82}$-POSS with a short PAA chain self-assemble into rather large ellipsoidal aggregates with a moderately uniform size, whereas POSS-PAA$_{140}$-POSS with a long PAA chain self-assembles into more spherical aggregates with a broad size distribution. These aggregates resemble the large compound micelles reported by Zhang and Eisenberg.

The unexpected ellipsoidal shape is attributed to the formation of layered crystals parallel to the major axis of the ellipsoids.

AUTHOR INFORMATION

Corresponding Author

*E-mail: wazhang@ecust.edu.cn (W.Z.); axel.mueller@uni-bayreuth.de (A.M.).

ACKNOWLEDGMENT

This work was supported by the National Natural Science Foundation of China (nos. 21074035 and 20804043). W.Z. also acknowledges support by the Alexander von Humboldt Foundation and the Fundamental Research Funds for the Central Universities.

REFERENCES

(1) Nathaniel, A. L.; Meuler, A. J.; Hillmyer, M. A. *Prog. Polym. Sci.* **2008**, *33*, 875–893.
(2) Hamley, I. W. *The Physics of Block Copolymers*; Oxford University Press: New York, 1998.
(3) Alexandridis, P.; Lindman, B. *Amphiphilic Block Copolymers: Self-Assembly and Applications*; Elsevier: Amsterdam, 2000.
(4) Abetz, V.; Simon, P. F. W. *Adv. Polym. Sci.* **2005**, *189*, 125–2125.
(5) Gohy, J. F. *Adv. Polym. Sci.* **2005**, *190*, 65–136.
(6) Hadjichristidis, N.; Iatrou, H.; Pitsikalis, M.; Pispas, S.; Avgeropoulos, A. *Prog. Polym. Sci.* **2005**, *30*, 725–782.
(7) Rodriguez-Hernandez, J.; Checot, F.; Gnanou, Y.; Lecommandoux, S. *Prog. Polym. Sci.* **2005**, *30*, 691–724.
(8) Darling, S. B. *Prog. Polym. Sci.* **2007**, *32*, 1152–1204.
(9) Teoh, S. K.; Ravi, P.; Dai, S.; Tam, K. C. *J. Phys. Chem. B* **2005**, *109*, 4431–4438.
(10) Korczagin, I.; Hempenius, M. A.; Fokkink, R. G.; Cohen Stuart, M. A.; Al-Hussein, M.; Bomans, P. H. H.; Frederik, P. M.; Vancso, G. J. *Macromolecules* **2006**, *39*, 2306–2315.
(11) Nikolic, M. S.; Olsson, C.; Salcher, A.; Kornowski, A.; Rank, A.; Schubert, R.; Frömsdorf, A.; Weller, H.; Förster, S. *Angew. Chem., Int. Ed.* **2009**, *48*, 2752–2754.
(12) Lichtenhan, J. D.; Schwab, J. J.; Feher, F. J.; Soulivong, D. U.S. Patent 5,942,638, 1999.
(13) Pielichowski, K.; Njuguna, J.; Janowski, B.; Pielichowski, J. *Adv. Polym. Sci.* **2006**, *201*, 225–296.
(14) Li, G. Z.; Wang, L. C.; Ni, H. L.; Pittman, C. U. *J. Inorg. Organomet. Polym.* **2001**, *11*, 123–154.
(15) Laine, R. M. *J. Mater. Chem.* **2005**, *15*, 3725–3744.
(16) Lee, A.; Xiao, J.; Feher, F. J. *Macromolecules* **2005**, *38*, 438–444.
(17) Cho, H. J.; Hwang, D. H.; Lee, J. I.; Jung, Y. K.; Park, J. H.; Lee, J.; Lee, S. K.; Shim, H. K. *Chem. Mater.* **2006**, *18*, 3780–3787.
(18) Chou, C. H.; Hsu, S. L.; Dinakaran, K.; Chiu, M. Y.; Wei, K. H. *Macromolecules* **2005**, *38*, 745–751.
(19) Kopesky, E. T.; Haddad, T. S.; Cohen, R. E.; McKinley, G. H. *Macromolecules* **2004**, *37*, 8992–9004.
(20) Abad, M. J.; Barral, L.; Fasce, D. P.; Williams, R. J. J. *Macromolecules* **2003**, *36*, 3128–3135.
(21) Mabry, J. M.; Vij, A.; Iacono, S. T.; Viers, B. D. *Angew. Chem., Int. Ed.* **2008**, *47*, 4137–4140.
(22) Xu, H. Y.; Kuo, S. W.; Lee, J. S. Y.; Chang, F. C. *Macromolecules* **2002**, *35*, 8788–8793.
(23) Knight, P. T.; Lee, K. M.; Qin, H.; Mather, P. T. *Biomacromolecules* **2008**, *9*, 2458–2467.
(24) Markovic, E.; Matisons, J.; Hussain, M.; Simon, G. P. *Macromolecules* **2007**, *40*, 4530–4534.
(25) Su, X. Y.; Guang, S. Y.; Xu, H. Y.; Liu, X. Y.; Li, S.; Wang, X.; Deng, Y.; Wang, P. *Macromolecules* **2009**, *42*, 8969–8976.
(26) Hottle, J. R.; Deng, J.; Kim, H. J.; Farmer-Creely, C. E.; Viers, B. D.; Esker, A. R. *Langmuir* **2005**, *21*, 2250–2259.
(27) Zheng, L.; Hong, S.; Cardoen, G.; Burgaz, E.; Gido, S. P.; Coughlin, E. B. *Macromolecules* **2004**, *37*, 8606–8611.
(28) Hirai, T.; Leolukman, M.; Hayakawa, T.; Kakimoto, M. A.; Gopalan, P. *Macromolecules* **2008**, *41*, 4558–4560.
(29) Pyun, J.; Matyjaszewski, K. *Chem. Mater.* **2001**, *13*, 3436–3448.
(30) Pyun, J.; Matyjaszewski, K.; Wu, J.; Kim, G. M.; Chun, S. B.; Mather, P. T. *Polymer* **2003**, *44*, 2739–2750.
(31) Drazkowski, D. B.; Lee, A.; Haddad, T. S.; Cookson, D. J. *Macromolecules* **2006**, *39*, 1854–1863.
(32) Drazkowski, D. B.; Lee, A.; Haddad, T. S. *Macromolecules* **2007**, *40*, 2798–2805.
(33) Miao, J.; Cui, L.; Lau, H. P.; Mather, P. T.; Zhu, L. *Macromolecules* **2007**, *40*, 5460–5470.
(34) Ni, Y.; Zheng, S. X. *Macromolecules* **2007**, *40*, 7009–7018.
(35) Kim, B. S.; Mather, P. T. L. *Macromolecules* **2006**, *40*, 9253–9260.
(36) Ohno, K.; Sugiyama, S.; Koh, K.; Tsujii, Y.; Fukuda, T.; Yamahiro, M.; Oikawa, H.; Yamamoto, Y.; Ootake, N.; Watanabe, K. *Macromolecules* **2004**, *37*, 8517–8522.
(37) Zhang, W. A.; Liu, L.; Zhuang, X. D.; Li, X. H.; Bai, J. R.; Chen, Y. *J. Polym. Sci., Part A: Polym. Chem.* **2008**, *46*, 7049–7061.
(38) Zhang, W. A.; Fang, B.; Walther, A.; Müller, A. H. E. *Macromolecules* **2009**, *42*, 2563–2569.
(39) Yu, X. Y.; Zhong, S.; Li, X. P.; Tu, Y. F.; Yang, S. G.; Horn, R. M. V.; Ni, C. Y.; Pochan, D. J.; Quirk, R. P.; Wesdemiotis, C.; Zhang, W. B.; Cheng, S. Z. D. *J. Am. Chem. Soc.* **2010**, *132*, 16741–16744.
(40) Zhang, W. A.; Müller, A. H. E. *Macromolecules* **2010**, *43*, 3148–3152.
(41) Wilhelm, N.; Zhao, C. L.; Wang, Y.; Xu, R.; Winnik, M. *Macromolecules* **1991**, *24*, 1033–1040.
(42) Zimm, B. H. *J. Chem. Phys.* **1948**, *16*, 1099.
(43) Chu, B. *Laser Light Scattering*, 2nd ed.; Academic Press: New York, 1991.
(44) Berne, B.; Pecora, R. *Dynamic Light Scattering*; Plenum Press: New York, 1976.
(45) Wu, C.; Xia, K. Q. *Rev. Sci. Instrum.* **1994**, *65*, 587–590.
(46) Zhang, J. Y.; Zhou, Y. M.; Zhu, Z. Y.; Ge, Z. S.; Liu, S. Y. *Macromolecules* **2008**, *41*, 1444–1454.
(47) Urbani, C. N.; Bell, C. A.; Whittaker, M. R.; Monteiro, M. J. *Macromolecules* **2008**, *41*, 1057–1060.
(48) Ciolacu, F. C. L.; Choudhury, N. R.; Dutta, N.; Kosior, E. *Macromolecules* **2007**, *40*, 265–272.
(49) Kaneshiro, T. L.; Wang, X. L.; Lu, Z. R. *Mol. Pharmaceutics* **2007**, *4*, 759–768.
(50) Zhang, L.; Eisenberg, A. *J. Am. Chem. Soc.* **1996**, *118*, 3168–3181.
(51) Zhang, L. F.; Eisenberg, A. *Macromolecules* **1996**, *29*, 8805–8815.
(52) Schilli, C.; Zhang, M.; Müller, A. H. E.; Rizzardo, E.; Thang, S. H.; Chong, Y. K.; Edwards, K.; Karlsson, G. *Macromolecules* **2004**, *37*, 7861–7866.
(53) Zhang, L.; Eisenberg, A. *Science* **1995**, *268*, 1728–1731.
(54) Zhou, Z. L.; Li, Z. B.; Ren, Y.; Hillmyer, M. A.; Lodge, T. P. *J. Am. Chem. Soc.* **2003**, *125*, 10182–10183.
(55) Lodge, T. P.; Hillmyer, M. A.; Zhou, Z. L. *Macromolecules* **2004**, *37*, 6680–6682.
(56) Floudas, G.; Fytas, G.; Pispas, S.; Hadjichristidis, N.; Pakula, T.; Khokhlov, A. R. *Macromolecules* **1995**, *28*, 5109–5118.
(57) Zaroslov, Y. D.; Fytas, G.; Pitsikalis, M.; Hadjichristidis, N.; Philippova, O. E.; Khokhlov, A. R. *Macromol. Chem. Phys.* **2005**, *206*, 173–179.
(58) Giannelis, E. P.; Krishnamoorti, R.; Manias, E. *Adv. Polym. Sci.* **1999**, *138*, 107–147.
(59) Waddon, A. J.; Coughlin, E. B. *Chem. Mater.* **2003**, *15*, 4555–4561.